$Pr_{0.5}Ba_{0.5}Co_{0.7}Fe_{0.25}Nb_{0.05}O_{3-\delta}$ as air electrode for solid oxide steam electrolysis cells

Ze-Tian Tao[a,b], Yan-Mei Jiang*[,b], Libin Lei [b], Fanglin Chen*[,b]

[a] *Key Laboratory for Advanced Technology in Environmental Protection of Jiangsu Province, Yancheng Institute of Technology, Yancheng, Jiangsu, China*

[b] *Department of Mechanical Engineering, University of South Carolina, Columbia, SC 29208, USA*

* *Corresponding authors. E-mail: chenfa@cec.sc.edu(F. Chen), yanmeij@mailbox.sc.edu (Y. M. Jiang)*

Abstract

$Pr_{0.5}Ba_{0.5}Co_{0.7}Fe_{0.25}Nb_{0.05}O_{3-\delta}$ (PBCFN) is synthesized and evaluated as air electrode for solid oxide steam electrolysis cells (SOECs). X-ray diffraction and TEM analysis show that PBCFN has a pure cubic perovskite structure with a lattice fringe spacing of 0.39 nm for the (110) planes. When the applied voltage is set at 1.3 V, a relatively high electrolysis current density of 470 mA cm^2 at 800°C is achieved for electrolyte-supported electrolysis cells with the cell configuration of $Sr_2Fe_{1.5}Mo_{0.5}O_6$ (SFM)–$Sm_{0.2}Ce_{0.8}O_2$ (SDC)/$La_{0.8}Sr_{0.2}Ga_{0.87}Mg_{0.13}O_3$ (LSGM)/SDC–PBCFN. In addition, there is no obvious degradation during the short-term stability test of the above cells at a constant electrolysis voltage of 1.3 V, indicating that PBCFN is a promising air electrode for SOECs.

Keywords: Air electrode materials, Chemical stability, Electrochemical performance, Perovskite structure, Solid oxide electrolysis cells

1. Introduction

Clean and renewable energy resources will play a pivotal role in achieving a sustainable global energy supply and combating the environmental issues associated with the ever increasing consumption of fossil fuels [1, 2]. Hydrogen has been regarded as an environmentally benign and highly efficient energy carrier because the emission product is water and the created high heat can also be utilized. H_2 can be produced from steam electrolysis from the solid oxide electrolysis cells (SOECs) under the driving external force of renewable electricity. To ensure success and large-scale deployment of the SOEC system, breakthroughs in the new electrode materials development are vital for the SOEC technology.

Ni-based cermets are the most studied and the state-of-the-art hydrogen electrode materials for SOECs due to their excellent electrical and catalytic properties [3]. However, they also face disadvantages such as poor redox stability, susceptible to vaporization and coarsening at a high temperature and humidity atmosphere [4-6]. Consequently, alternative hydrogen electrode material such as $Sr_2Fe_{1.5}Mo_{0.5}O_6$ (SFM) has recently been explored due to its enhanced redox cycling ability and relatively high melting point [7–9].

Considering the air electrode materials, the performance of electrolysis cells is highly related with the sluggish rate of oxygen evolution reaction (OER). In solid oxide fuel cells (SOFCs), the materials with mixed ionic and electronic conducting (MIEC) ability are fabricated to enhance the triple-phase boundary (TPB), thus the polarization resistance is reduced. For SOECs, the cell catalytic ability and performance can also be highly improved by using MIECs as the air electrode. Among the air electrode materials developed for SOECs, $La_xSr_{1-x}Co_yFe_{1-y}O_3$ (LSCF), which has been widely studied in oxygen-ion conducting SOFC (O-SOFC), has also been applied in SOECs for its high electronic and ionic conductivities [10, 11]. However, the relatively slow kinetics of oxygen dissociation-absorption process has been proved to limit the performance of LSCF as air electrode material for SOFCs [12]. Recently, $PrBaCo_2O_6$ series materials have been studied as air electrode materials for SOFCs and shows excellent cell performance because of its high catalytic ability [13]. In addition, it has been proved that the substitution of a small amount of Fe for Co can slightly improve the catalytic performance [14]. However, the volatility of Co element limits the operation life. On the other hand, Nb doping has been proved to be an effective way to improve the electrode stability for cobaltite perovskite by several groups. [15-20]

In this study, Nb and Fe doped $Pr_{0.5}Ba_{0.5}Co_{0.7}Fe_{0.25}Nb_{0.05}O_{3-\delta}$ (PBCFN) is synthesized and characterized as air electrode material for SOECs based on $La_{0.8}Sr_{0.2}Ga_{0.87}Mg_{0.13}O_3$ (LSGM) electrolyte. XRD and TEM are used to characterize the crystal structure of the synthesized PBCFN powders. Cell voltage-current relationship as well as the impedance spectra of the cells is evaluated in both SOFC and SOEC modes. In addition, the short-term stability of the SOECs is also investigated.

2. Experimental

2.1 Powder Syntheses

The PBCFN powders were synthesized via a wet Pechini method. All of the starting chemicals, $Pr(NO_3)_3 \cdot 6H_2O$(99.9%), $BaCO_3$(99%), $Co(NO3)_4 \cdot 4H_2O$(99%), $C_4H_4NNbO_9$ (99.9%), are analytical reagents purchased from Sigma-Aldrich. Appropriate amount of the starting materials were dissolved in EDTA-NH_3 aqueous solution under the conditions of heating and stirring. Appropriate amount of citric acid was subsequently added into the solution to form sol complexes. The molar ratio was set at 1: 1.5: 1 for EDTA: citric acid: metal cations. The mixture was heated under stirring and became gel which ignited to flame and resulted in an ash-like material. The as-prepared material was calcined in air at 1100 °C for 10 hours to obtain final powders. In addition, the SFM powders were obtained through wet Pechini method as described in our previous paper [21]. $La_{0.8}Sr_{0.2}Ga_{0.87}Mg_{0.13}O_3$ (LSGM) electrolyte powders were purchased from FuelCell Materials Inc.

2.2 Fabrication of single cells

The electrolyte supported steam electrolysis cells with the configuration of SFM–SDC/LSGM/SDC–PBCFN were prepared for electrochemical performance evaluations. LSGM powders were pressed under uniaxially pressure to LSGM pellets with a diameter of 13 mm and then sintered at 1500 °C for 5 hours to obtain dense LSGM electrolyte disks. The composite electrode slurries of PBCFN/SDC and SFM/SDC were prepared by mixing SDC powders with the corresponding electrode powders at a weight ratio of 30:70 with ink vehicle purchased from FuelCell Materials Inc. The electrode slurries were then screen-printed on the LSGM electrolyte surface in symmetric positions with an area of 0.3 cm^2 and calcined at 1000 °C for 3 h to form porous electrode. Ag paste was painted on the electrode surface as a current collector.

2.3 Characterization

The phase structures of the PBCFN powders were studied by X-ray diffractometer (XRD) using Cu-Ka radiation (1.5418 Å) at 40 kV and 40 mA. The crystal structure was further observed through TEM to establish the lattice fringe spacing. The cross-sectional microstructure of the single cells andwas observed by scanning electron microscope (SEM, Zeiss Ultra Plus FESEM).

The prepared single cells were sealed in a home-made testing system using an electrical conductive paste (DAD-87, Shanghai Research Institute of Synthetic Resins, China). Humidified hydrogen with various steam concentrations (from 3%- 42%) which was controlled by heating water to a certain temperature and then feeding into the hydrogen electrode chamber at a flow rate of 30 mL min^{-1}, while the air electrode side was exposed to ambient air. The mass flow rate of H_2 was controlled by using a digital mass flow controller (APEX, AlicatScientific) and the actual water partial pressure was determined using an on-line humidity sensor (HMP 337, Vaisala). Electrochemical performance of electrolysis cell including current density-voltage (I-V) and impedance spectra was measured on an electrochemical test system (Versa STAT 3-400, Princeton Applied Research, USA).

3. Result and discussion

Figure 1 shows the XRD pattern of the $Pr_{0.5}Ba_{0.5}Co_{0.7}Fe_{0.25}Nb_{0.05}O_{3-\delta}$ sample obtained after calcination at 1100 °C for 10 h in air. The sharp peaks located at 22.9°, 32.6°, 40.2°, 46.8°, 52.7°, 58.2°, 68.3°, 73.1°, and 77.7° can be readily indexed to the (110), (200), (211), (220), (310), (222), (400), (411), and (420) diffractions, respectively, with a cubic structure (space group Pm-3m). This indicates that further moderate substitution of Fe by Nb in $PrBaCoFeO_{5+\delta}$ materials does not change their phase structure, while the lattice parameter (0.39nm) increases slightly caused *[22]* by the larger ionic radii of $Nb^{4+}/^{5+}$ (0.068 (HS)/0.064(LS) nm) compared to those of $Fe^{3+}/^{4+}$ (0.0645 (HS)/0.0585 (LS) nm).

To identify more crystal structure information, $Pr_{0.5}Ba_{0.5}Co_{0.7}Fe_{0.25}Nb_{0.05}O_{3-\delta}$ sample was characterized by TEM observation (Figure 2a and b). Figure 2a shows a typical bright-field TEM image of single solid nanoparticle. The corresponding high resolution TEM image (Figure

2b) demonstrates the presence of crystalline fringes, corresponding to the (110) plane of the cubic single perovskite structure, with a lattice fringe spacing of 0.39 nm, which is in agreement with that of the XRD analysis (d_{110} = 0.39 nm). Single perovskite phase has the advantages of intrinsic 3D diffusion channels. The channels facilitate the fast penetration of oxygen ions into the $Pr_{0.5}Ba_{0.5}$ $(Co_{0.7}Fe_{0.25}Nb_{0.05})$ $O_{3-\delta}$ lattice (Figure 2b inset).

Figure 3 presents the microstructures of the typical cross-section of the single electrolysis cell with configuration of PBCFN-SDC/LSGM/SFM-SDC. From figure 3(a), we can find that the electrolyte is about 450um. The thick electrolyte may lead to high ohmic resistance of the total cell, thus lowering the cell performance, which can be improved by further reducing the electrolyte thickness in future work. In addition, the electrode is attached very well with the electrolyte without any obvious cracks from the enlarged morphology in figure 3(b).

Fig. 4a shows the current density-cell voltage (I–V) curves and power density-cell voltage (P-V) curves of the electrolysis cells in SOFC mode exposing the anode to a 3% H_2O–97% H_2 atmosphere and the cathode to ambient air at different temperatures. The OCVs at 800 and 850°C are 1.008 and 1.000 V, respectively, corresponding to the minimum cell voltage required to start the water splitting process. Moreover, the maximum power densities (MPDs) of single cells at 800 and 850°C are 0.406W cm^{-2} and 0.246W cm^{-2}, respectively. From the figure, we can find the cell performance increases with the operating temperature. In addition, the cell resistances are also investigated by the impedance spectra in figure 4b. The Rp calculated from the real axis between low frequency and high frequency significantly decreases with the increase of the temperature, typically from 0.52 Ω cm^2 at 800 °C to 0.31 Ω cm^2 at 850 °C. Meanwhile, the ohmic resistance occupies a great part of the total resistance by comparing the impedance spectra, particularly at the low operating temperature, showing the cell performance can be significantly improved by reducing electrolyte thickness.

Figure 5 presents the I-V curves of the single cell in electrolysis mode exposing the cathode to an atmosphere of 3% H_2O–97% H_2. From the figure, it is obvious that the absolute current densities increase with the increase of the operation temperature and applied voltage. As shown in Figure 5, the current densities are -0.41 A cm^{-2} and -0.65 A cm^{-2} at 800 and 850°C, respectively when the applied voltage is set at 1.3V. In addition, single cells in electrolysis mode at different steam concentrations are also observed at 800°C and shown in Figure 6. The current densities are highly related with the steam concentrations. For example, when the applied voltage is at 1.3V, the current density is -0.41 A cm^{-2} under steam concentrations of 3% while it increases to -0.53 A cm^{-2} when the steam concentration is 42%. The cell performance is also compared with the electrolysis cells with different electrodes reported in the literature and shown in Table 1 [10, 23-28]. As can be seen in the table, the electrochemical performance of PBCFN is comparable to that of $Ba_{0.9}Co_{0.7}Fe_{0.2}Nb_{0.1}O_{3-\delta}$ (BCFN) and SFM electrode and better than most other air electrode materials such as $(La_{0.75}Sr_{0.25})_{0.95}MnO_3$ (LSM) and $La_xSr_{1-x}Co_yFe_{1-y}O_3$ (LSCF).

In order to further study the electrolysis cell, the impedance spectra at various applied voltages under the steam concentration of 30% at 800°C shown in Figure 7. An equivalent circuit (inserted in the figure) which consists of R_0, L and CPE-R_H, CPE-R_L parallels in serial connection is applied to fit the impedance spectra using Zview program. In general, the impedance spectra observed in this study are consisted of the ohmic resistance and polarization resistance. The ohmic resistances are almost the same at different applied voltages while the polarization resistances show significant differences, being about 0.99Ω cm^2 in the SOFC mode (0.7V), 0.19Ω cm^2 under 1.3V and 0.49Ω cm^2 under OCV in the SOEC mode. The EIS profiles feature a depressed arc shape, which consists of two arcs associated with two different mechanisms. The high frequency arc is corresponding to the charge transfer while the low frequency arc is dominated by the mass transfer of the solid oxide electrolyser[29]. When the EIS is tested in the SOEC mode, the electrode reactions such as surface diffusion of O^{ad-} will be highly improved thus enhancing the electrode process and decreasing the electrode polarization resistance at the high cell voltage [30].

To investigate the stability of SFM–SDC/LSGM/SDC–PBCFN electrolysis cells at 850°C, the cells are operated at 1.3V with the cathode exposed to 3% H_2O–97% H_2 for 10h, as shown in Figure 8. During the operation life, the current density is slightly decreased and then stable at -495mA cm^{-2}, indicating that PBCFN is relatively a stable catalyst and the cell using this catalyst as anode can obtain stable operation performance under the operating conditions of high temperature, because SFM had been proven to be a stable anode material under the electrolysis process in the previous study [10].

4. Conclusion

Stable perovskite structure PBFCN cathode is synthesized and applied on the solid oxide steam electrolysis cells with LSGM as electrolyte and SFM as the anode material. The doping of Nb in the cathode has improved the phase stability of PBCF and thus enhanced the electrolysis cell stability under the operation conditions. The electrochemical test showed that the cell performance can obtain a high current density of 0.53 A cm^{-2} when the steam concentrations is 42% with the applied voltage of 1.3V. Moreover, the relationship of current densities and operation temperatures are also observed and tested. Consequently, the SOEC with PBCFN cathode shows stable and good performance at electrolysis mode (applied voltage is set at 1.3V) for 10h, showing great potential for further research.

Acknowledgements

This work is supported by the National Natural Science Foundation of China (Grant Number: 21406190), Natural Science Foundation of the Higher Education Institutions of Jiangsu Province (No. 18KJA430017) and the U.S. National Science Foundation (DMR–1832809).

Reference

[1] M.I. Hoffert, K. Caldeira, G. Benford, et al. Advanced Technology Paths to Global Climate Stability: Energy for a Greenhouse Planet, Science, 2002, **295**: 981-987.

[2] K. Xie, Y.Q. Zhang, G.Y. Meng, J.T.S. Irvine. Direct synthesis of methane from CO_2/H_2O in an oxygen-ion conducting solid oxide electrolyser,Energy Environ. Sci., 2011, **4**: 2218-2222.

[3] T. Liu, Y. Wang, Y. Zhang, S. Fang, L. Lei, C. Ren and F. Chen. Steam electrolysis in a solid oxide electrolysis cell fabricated by the phase-inversion tape casting method, *Electrochem. Commun.*, 2015, **61**:106–109.

[4] Y. Wang and C. Xia. Nano-structural effect on SOFC durability. In: Dennis Y.C. Leung, Jin Xuan, editors. Micro & Nano-Engineering of Fuel Cells, CRC Press; 2015, p. 181–210.

[5] D. Sarantaridis and A. Atkinson. Redox cycling of Ni-based solid oxide fuel cell anodes: a review, *Fuel Cells*, 2007, **7**: 246–258.

[6] H. Yokokawa, K. Yamaji, M. Brito, H. Kishimoto and T. Horita. General considerations on degradation of Solid Oxide Fuel Cell anodes and cathodes due to impurities in gases, *J. Power Sources*, 2011, **196**: 7070–7075.

[7] Y. Wang, T. Liu, S. Fang and F. Chen. Syngas production on a symmetrical solid oxide H_2O/CO_2 co-electrolysis cell with $Sr_2Fe_{1.5}Mo_{0.5}O_6$–$Sm_{0.2}Ce_{0.8}O_{1.9}$ electrodes, *J. Power Sources*, 2016, **305**: 240–248.

[8] Y. Wang, T. Liu, S. Fang, G. Xiao, H. Wang and F. Chen. A novel clean and effective syngas production system based on partial oxidation of methane assisted solid oxide co-electrolysis process, *J. Power Sources*, 2015, **277**: 261–267.

[9] Q. Liu, X. Dong, G. Xiao, F. Zhao and F. Chen. A novel electrode material for symmetrical SOFCs, *Adv. Mater.*, 2010, **22**: 5478–5482.

[10] Y. Wang, T. Liu, M. Li, C. Xia, B. Zhou and F. Chen. Exsolved Fe–Ni nano-particles from $Sr_2Fe_{1.3}Ni_{0.2}Mo_{0.5}O_6$ perovskite oxide as a cathode for solid oxide steam electrolysis cells, *J. Mater. Chem. A*, 2016, **4**: 14163-14169.

[11]Z. Pan, Q. Liu, M. Ni, R. Lyu, P. Li, S.H. Chan. Activation and failure mechanism of $La_{0.6}Sr_{0.4}Co_{0.2}Fe_{0.8}O_{3-\delta}$ air electrode in solid oxide electrolyzer cells under high-current electrolysis, *Int. J. Hydrogen Energy*, 2018, **43**:5437-5450.

[11] G. Li, B. He, Y. Ling, J. Xu, L. Zhao. Highly active YSB infiltrated LSCF cathode for proton conducting solid oxide fuel cells, *Int. J. Hydrogen Energy*, 2015, 40:13576-13582.

[13] S.L. Pang, W.Z. Wang, T. Chen, Y.G. Wang, K.J. Xu, X.Q. Shen, X.M. Xi, J.M .Fan. The effect of potassium on the properties of $PrBa_{1-x}Co_2O_{5+\delta}$(x=0.00-0.10) cathodes for intermediate-temperature solid oxide fuel cells. Int. J. Hydrogen Energy 2016; 41:13705-13714.

[14] Y.N. Kim, J.H. Kim, A. Manthiram. Effect of Fe substitution on the structure and properties of $LnBaCo_{2-x}FexO_{5+\delta}$ (Ln= Nd and Gd) cathodes, J. Power Sources, 2010, 195(19) 6411-6419.

[15] C. Zhu, X. Liu, C. Yi, L. Pei, D. Yan, J. Niu, D. Wang, W. Su. Novel $BaCo_{0.7}Fe_{0.3-y}Nb_yO_{3-\delta}$ (y= 0–0.12) as a cathode for intermediate temperature solid oxide fuel cell, *Electrochem Commun*, 2009, **11(5)**: 958-961.

[16] Z. Liu, L. Cheng, M. Han. A-site deficient $Ba_{1-x}Co_{0.7}Fe_{0.2}Ni_{0.1}O_{3-\delta}$ cathode for intermediate temperature SOFC, *J. Power Sources*, 2011, **196(2)**: 868-871.

[17] Z. Yang, C. Yang, C. Jin, M. Han, F. Chen. $Ba_{0.9}Co_{0.7}Fe_{0.2}Nb_{0.1}O_{3-\delta}$ as cathode material for intermediate temperature solid oxide fuel cells, *Electrochem Commun*, 2011, **13(8)**: 882-885.

[18] Z. Yang, C. Yang, B. Xiong, M. Han, F. Chen. $BaCo_{0.7}Fe_{0.2}Nb_{0.1}O_{3-\delta}$ as cathode material for intermediate temperature solid oxide fuel cells, *J. Power Sources*, 2011, **196(22)**: 9164-9168.

[19] M. Saccoccio, C.L. Jiang, Y. Gao, D.J. Chen, F. Ciucci. Nb-substituted $PrBaCo_2O_{5+\delta}$ as a cathode for solid oxide fuel cells: A systematic study of structural, electrical, and electrochemical properties. Int. J. Hydrogen Energy 2017; 42:19204-19215.

[20] Z. Yang, C. Jin, C. Yang, M. Han, F. Chen. $Ba_{0.9}Co_{0.5}Fe_{0.4}Nb_{0.1}O_{3-\delta}$ as novel oxygen electrode for solid oxide electrolysis cells, Int. J. Hydrogen Energy, 2011, **36(18)**:11572-11577.

[21] G. Xiao, Q. Liu, F. Zhao, L. Zhang, C. Xia and F. Chen. $Sr_2Fe_{1.5}Mo_{0.5}O_6$ as Cathodes for Intermediate-Temperature Solid Oxide Fuel Cells with $La_{0.8}Sr_{0.2}Ga_{0.87}Mg_{0.13}O_3$ Electrolyte, *J. Electrochem. Soc.*, 2011, **158**: B455–B460.

[22] J. Zou, J. Park, B. Kwak, H.Yoon, J. Chung. Effect of Fe doping on $PrBaCo_2O_{5+\delta}$ as cathode for intermediate-temperature solid oxide fuel cells, Solid State Ionics, 2012, 206:112-119.

[23] Q. Liu, C. Yang, X. Dong and F. Chen. Perovskite $Sr_2Fe_{1.5}Mo_{0.5}O_{6-\delta}$ as electrode materials for symmetrical solid oxide electrolysis cells, Int. J. Hydrogen Energy, 2010, 35, 10039–10044.

[24] C. Yang, Z. Yang, C. Jin, M. Liu and F. Chen. High performance solid oxide electrolysis cells using $Pr_{0.8}Sr_{1.2}(Co, Fe)_{0.8}Nb_{0.2}O_{4+\delta}$–Co–Fe alloy hydrogen electrodes, Int. J. Hydrogen Energy, 2013, 38, 11202–11208.

[25] C. Yang, A. Coffin and F. Chen. High temperature solid oxide electrolysis cell employing porous structured $(La_{0.75}Sr_{0.25})_{0.95}MnO_3$ with enhanced oxygen electrode performance, Int. J. Hydrogen Energy, 2010, 35, 3221–3226.

[26] G. Tsekouras and J. T. Irvine. The role of defect chemistry in strontium titanates utilised for high temperature steam electrolysis, J. Mater. Chem., 2011, 21, 9367–9376.

[27] S. Xu, D. Dong, Y. Wang, W. Doherty, K. Xie, Y. Wu. Perovskite chromates cathode with resolved and anchored nickel nano-particles for direct high-temperature steam electrolysis, J. Power Sources, 2014, 246, 346–355.

[28] S. Kim, K. Kim, G. Choi. A novel solid oxide electrolysis cell (SOEC) to separate anodic from cathodic polarization under high electrolysis current, Int. J. Hydrogen Energy, 2015, 40, 9032-9038.

[29] L. Zhang, S.P. Jiang, W. Wang, Y.J. Zhang. NiO/YSZ, anode-supported, thin-electrolyte, solid oxide fuel cells fabricated by gel casting, J. Power Sources 170 (2007) 55.

[30] S. Li, R. Yan, G. Wu, K. Xie, J. Cheng. Composite oxygen electrode LSM-BCZYZ impregnated with Co3O4 nanoparticles for steam electrolysis in a proton-conducting solid oxide electrolyzer, Int. J. Hydrogen Energy, 2013, 38, 14943-14951.

Table 1. Cell performance of solid oxide electrolysis cells reported in literatures.

		Electrochemical performance		
Cell configuration	Test conditions	i @ 1.3 V (A cm^{-2})	R @ OCV (Ω cm^2)	Ref.
SFM/LSGM/SFM	40% H_2O–60% H_2, 800°C	0.48	0.68	23
K-PSCFN-CFA/LSGM/BCFN	40% H_2O–60% H_2, 800°C	0.75	0.67	24
Ni–YSZ/YSZ/YSZ–LSM	50% H_2O–50% H_2, 800°C	0.3	1.0	25
LST/YSZ/YSZ–LSM	47% H_2O–50% N_2–3% H_2, 900°C	0.065	1.7	26
SFM–SDC/ LCO/LSGM/SDC–LSCF	42% H_2O–58% H_2, 850°C	0.64	0.44	10
LSCNNi-YSZ/YSZ/LSM-YSZ	3% H_2O–Ar–5% H_2, 800°C	0.031	4.2	27
Ni–YSZ/YSZ/YSZ–LSCF	40% H_2O–60% H_2, 800°C	0.61	0.42	28
SFM–SDC/ LSGM/SDC–PBCFN	3% H_2O–97% H_2, 800°C 42% H_2O–58% H_2, 800°C 3% H_2O–97% H_2, 850°C	0.41 0.53 0.65	0.51 0.48 0.30	This work

K-PSCFN-CFA: K- $Pr_{0.4}Sr_{0.6}Co_{0.2}Fe_{0.7}Nb_{0.1}O_{3-\delta}$–Co-Fe Alloy; BCFN: $Ba_{0.9}Co_{0.7}Fe_{0.2}Nb_{0.1}O_{3-\delta}$;YSZ: Yttria stabilized zirconia; LSM: Strontium doped lanthanum manganite; LST: $La_{0.3}Sr_{0.7}TiO_{3+\delta}$; LCO: $La_{0.5}Ce_{0.5}O_{1.5}$; LSCNNi: $(La_{0.75}Sr_{0.25})_{0.95}(Cr_{0.8}Ni_{0.2})_{0.95}Ni_{0.05}O_{3-\delta}$

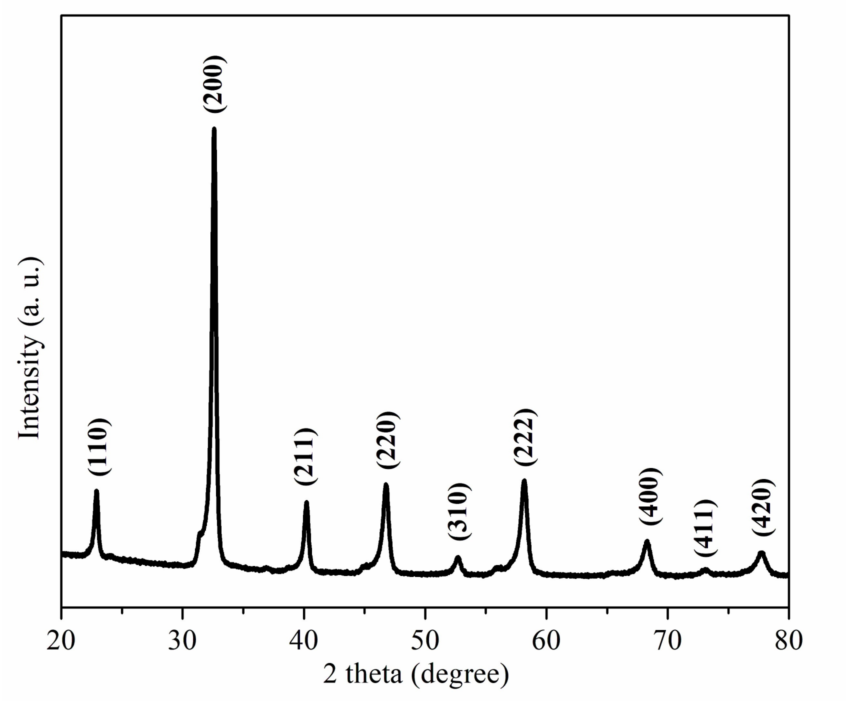

Figure 1. XRD pattern of the $Pr_{0.5}Ba_{0.5}$ $(Co_{0.7}Fe_{0.25}Nb_{0.05})$ $O_{3-\delta}$ sample after calcination at 1100 °C for 10 h in air.

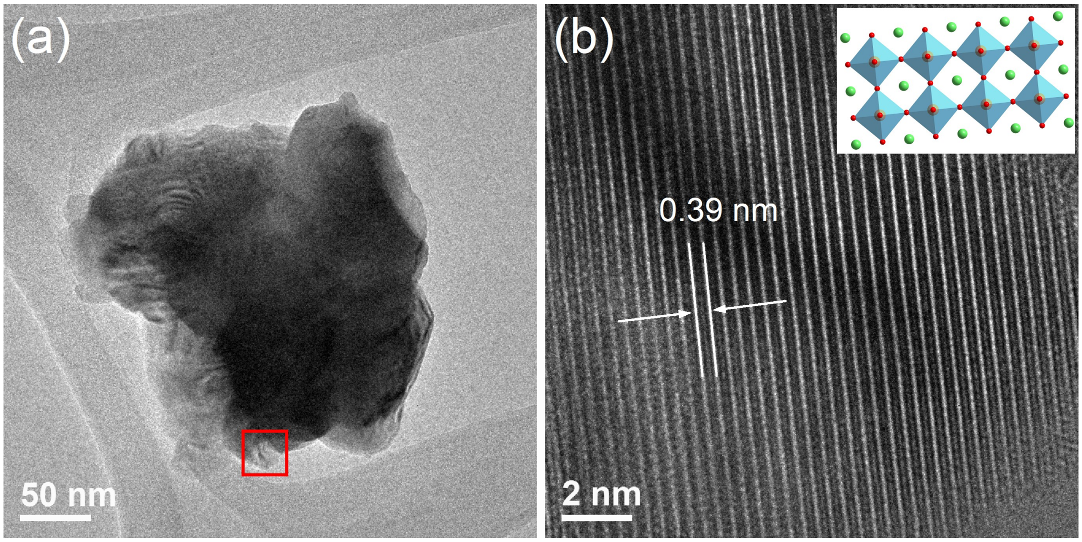

Figure 2. (a) TEM image of the $Pr_{0.5}Ba_{0.5}$ $(Co_{0.7}Fe_{0.25}Nb_{0.05})$ $O_{3-\delta}$. (b) Partial enlarged details of the part of red box in Figure 2a. The inset in b shows the corresponding crystal structure of cubic perovskite in projection along [100], expanded view of the framework built on Co/Fe/NbO_6 octahedra, with Pr/Ba ions in green.

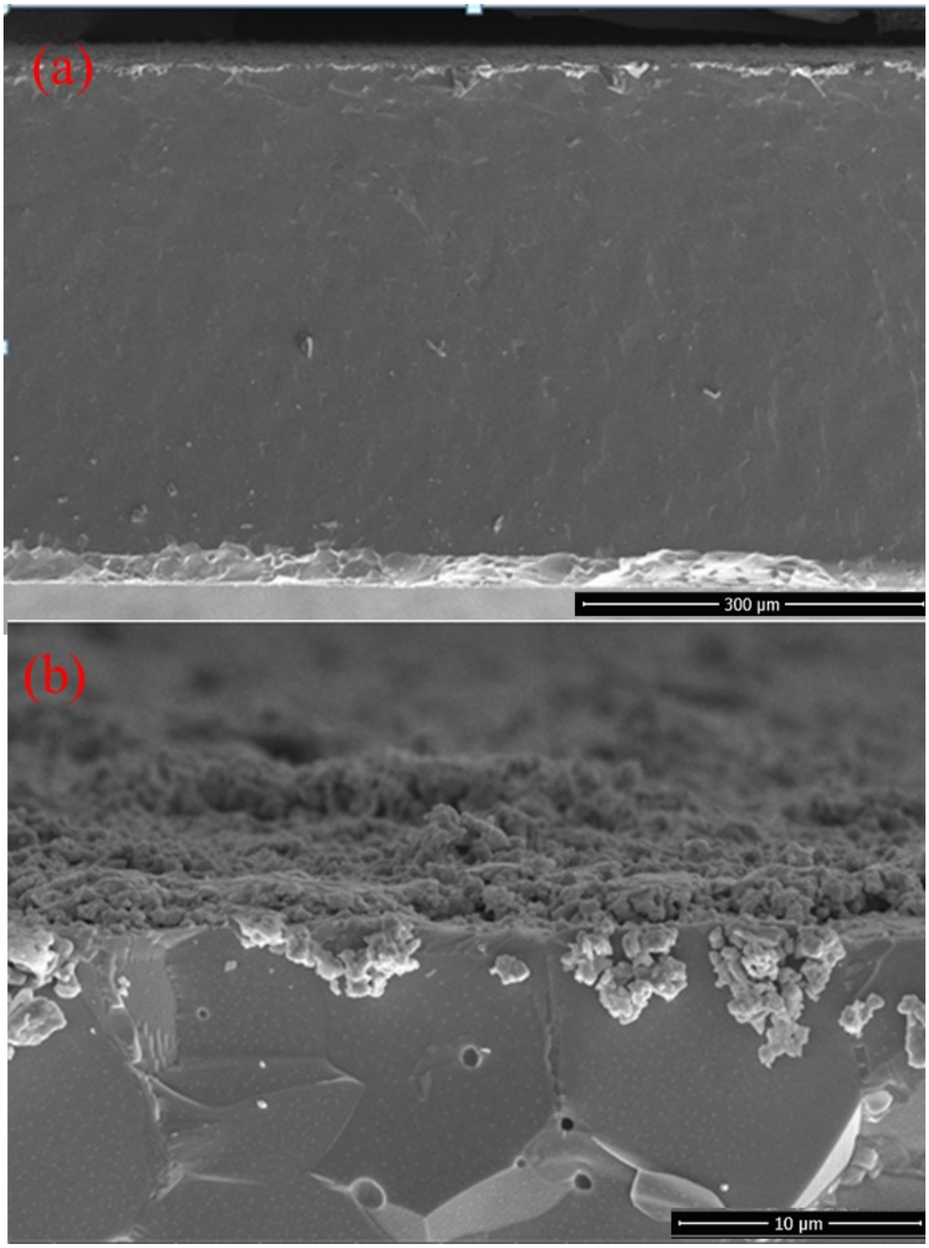

Figure 3. The cross-section morphology of the assembled single cells (a) and enlarged morphology of LSGM electrolyte (b).

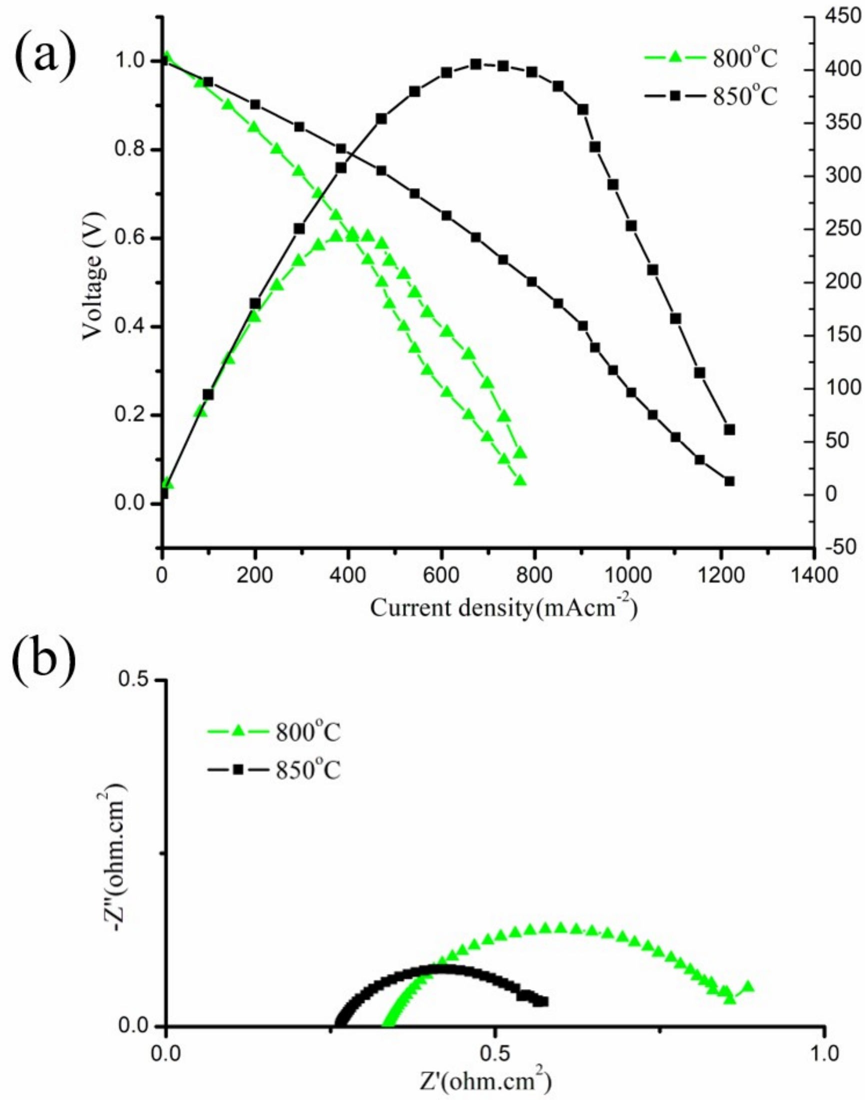

Figure 4. I-V Curves and impedance spectrum of the single cell tested at different temperatures in SOFC mode.

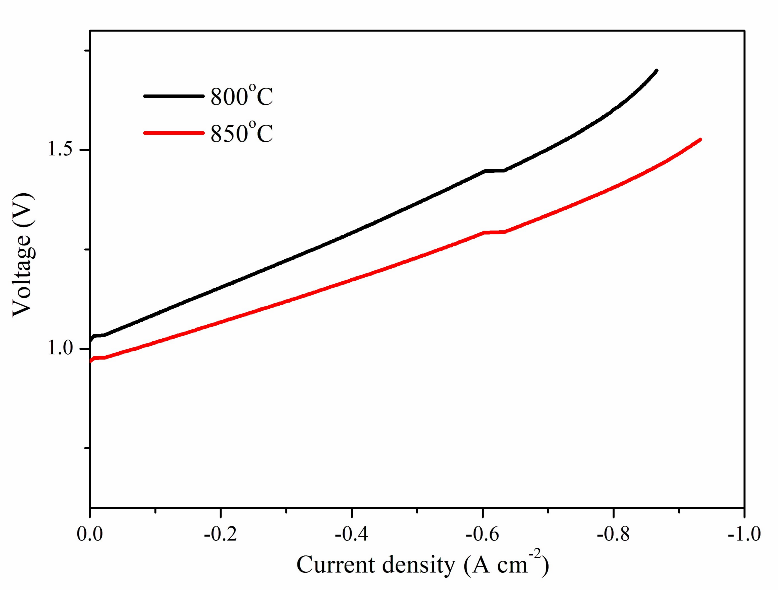

Figure 5. I-V curves of the single electrolysis cell recorded under the atmosphere of 3% H_2O–97% H_2.

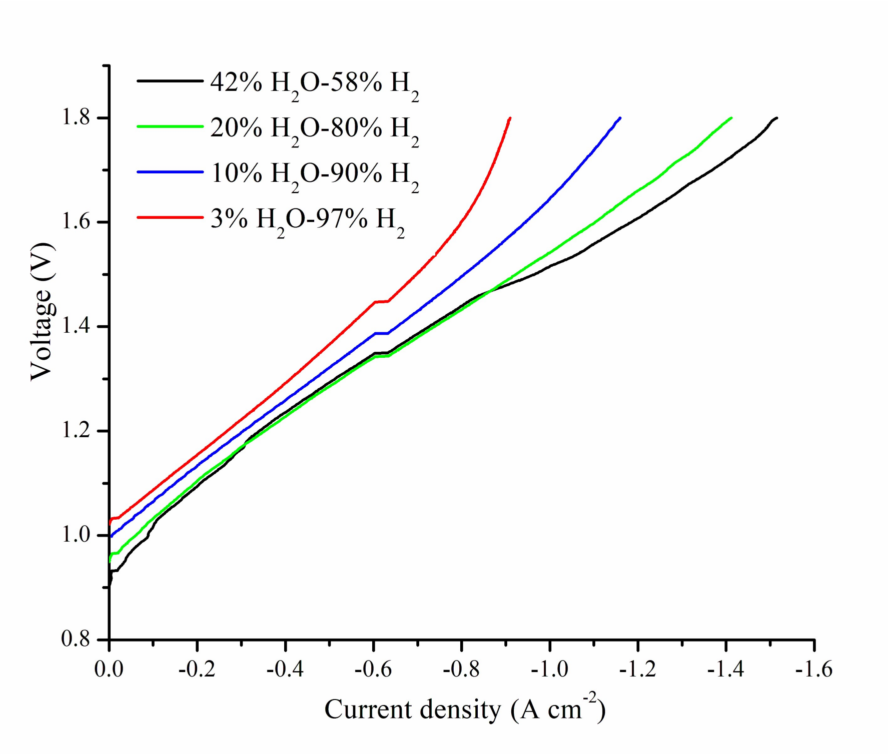

Figure 6. I-V curves of the single electrolysis cell under different steam concentrations at 800°C.

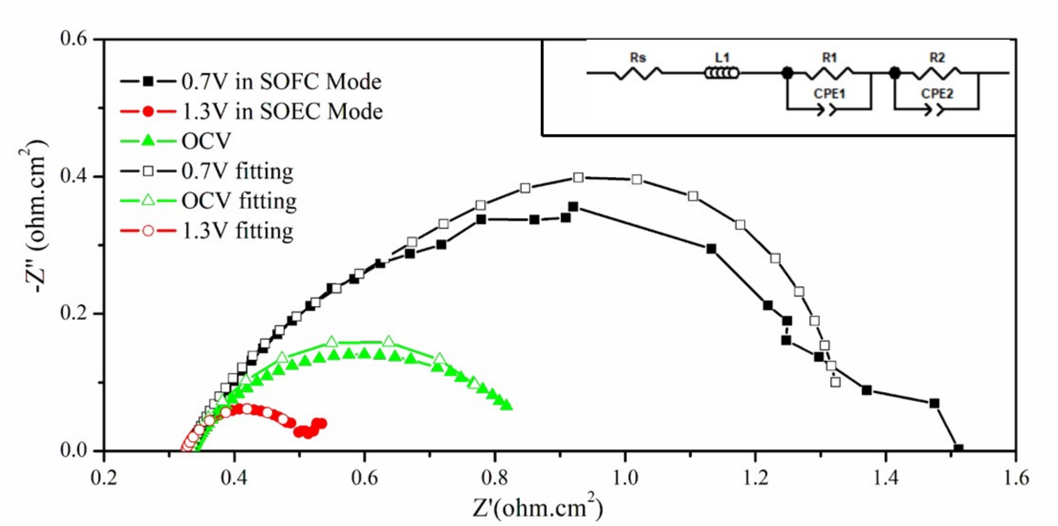

Figure 7. The impedance spectra of the single electrolysis cell operated under the steam concentration of 30% at 800 °C with different applied voltages.

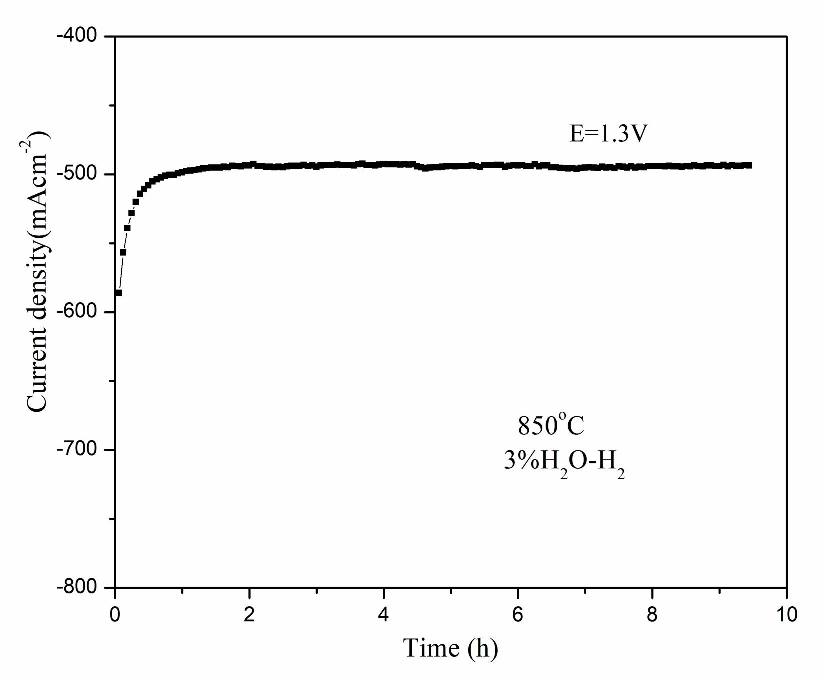

Figure 8. Time dependence of the cell voltage for the electrolysis cell measured at a constant voltage of 1.3V at 850°C under the conditions of 3% H_2O–97% H_2.